



Phosphorus controls on the formation of vivianite versus green rust under anoxic conditions

Yijun Xiong^{a,*}, Romain Guilbaud^b, Caroline L. Peacock^a, Michael D. Krom^{a,c},
Simon W. Poulton^a

^a School of Earth and Environment, University of Leeds, Leeds LS2 9JT, UK

^b Géosciences Environnement Toulouse, CNRS, 31400 Toulouse, France

^c Morris Kahn Marine Station, Charney School of Marine Sciences, Haifa University, Rehov Aba Koushy, Haifa, Israel

ARTICLE INFO

Associate editor: Caroline P. Slomp

Keywords:

Phosphorus cycling
Vivianite
Green rust
Mineral formation
Modern anoxic settings
Earth history

ABSTRACT

The formation of green rust (GR; a mixed ferric/ferrous hydroxide) and vivianite (ferrous phosphate) are likely to have exerted a major control on phosphorus (P) cycling in ancient anoxic oceans. However, the factors that influence the formation of these minerals under different chemical conditions are poorly constrained, which limits understanding of the pathways that ultimately result in P drawdown and retention in anoxic sediments. This, in turn, limits understanding of P cycling in anoxic oceans and hence potential productivity feedbacks. Here we explore the effect of dissolved P concentration on the formation of sulfate GR ($\text{Fe}_2^{\text{III}}\text{Fe}_3^{\text{II}}(\text{OH})_{12}\text{SO}_4$) versus vivianite ($\text{Fe}_3^{\text{II}}(\text{PO}_4)_2 \cdot 8\text{H}_2\text{O}$) under anoxic conditions. Our results show that at low dissolved P concentrations and with P:Fe(II) molar ratios <1:30, P drawdown is effectively controlled by interlayer anion exchange and adsorption onto GR species, via the formation of amorphous Fe-P precursors. Such precursors may delay the precipitation of crystalline GR, but vivianite was not detected under these conditions. At higher dissolved P concentrations and P:Fe(II) ratios, GR also forms. However, the GR formed under these conditions rapidly dissolves, likely forming amorphous ferric hydroxides together with dissolved Fe(II) and phosphate, with the dissolved species subsequently reacting to form crystalline vivianite. Our observations agree with studies showing the water column formation of GR in modern oligotrophic, anoxic Fe-rich (ferruginous) settings, and provide support for a major role for GR in controlling P cycling in ancient oligotrophic ferruginous oceans. By contrast, in more productive ancient anoxic settings, enhanced redox-controlled P recycling and/or increased weathering inputs would have led to higher dissolved P concentrations in the water column and sediments. Our observations show that such conditions ultimately promote the formation of vivianite, which would have exerted a limiting control on the extent of P recycling in ancient, more productive settings, via the long-term fixation of P in the sediments.

1. Introduction

Understanding the cycling of P in anoxic oceans and sediments is important in terms of evaluating controls on Earth's oxygenation history. This is because P is the ultimate limiting nutrient on geologic timescales (Tyrrell, 1999) and thus plays a fundamental role in primary production, the burial flux of organic carbon, and hence atmospheric oxygenation (e.g., Laakso and Schrag, 2014; Reinhard et al., 2017; Canfield et al., 2020; Guilbaud et al., 2020; Alcott et al., 2022). Unlike the well-oxygenated conditions that characterize most of the modern ocean, anoxic conditions are reported to have been considerably more

prevalent throughout much of Earth's history (e.g., Jenkyns, 2010; Poulton and Canfield, 2011). However, the precise nature of anoxia, including whether ferruginous (anoxic and iron-containing) or euxinic (anoxic and sulfide-containing) conditions occurred in the sediments and water column, would have been a crucial factor controlling P bioavailability, via redox-dependent chemical and biological controls on P recycling versus fixation in the sediment (e.g., Poulton, 2017; Guilbaud et al., 2020).

Under ferruginous water column conditions, dissolved P may be efficiently drawn down from the water column through co-precipitation with, and adsorption onto, Fe (oxyhydr)oxide minerals (Bjerrum and

* Corresponding author.

E-mail address: earyx@leeds.ac.uk (Y. Xiong).

<https://doi.org/10.1016/j.gca.2023.04.032>

Received 9 January 2023; Accepted 27 April 2023

Available online 3 May 2023

0016-7037/© 2023 The Authors. Published by Elsevier Ltd. This is an open access article under the CC BY license (<http://creativecommons.org/licenses/by/4.0/>).

Canfield, 2002; Konhauser et al., 2007b; Jones et al., 2015). Depending on organic carbon loading and the rate of microbial Fe reduction, P may subsequently be released back into the water column. This P release is further augmented when sulfide is produced in the sediment (via microbial sulfate reduction), through both the reductive dissolution of Fe (oxyhydr)oxide minerals by hydrogen sulfide (e.g., Krom and Berner, 1981; Pyzik and Sommer, 1981; Peiffer et al., 1992; Poulton, 2003; Poulton et al., 2004), and by preferential release of P during organic matter remineralisation (e.g., Ingall et al., 1993; Van Cappellen and Ingall, 1994; Ingall and Jahnke, 1997; Slomp et al., 2004). However, the diffusive flux of dissolved P to the water column may be balanced, to a certain extent, by its re-adsorption onto sinking Fe particles in the ferruginous water column (Dellwig et al., 2010). The depositional flux of Fe minerals under such conditions may therefore ultimately result in enhanced P fixation in marine sediments, leading to a negative feedback on primary production (e.g., März et al., 2008; Poulton et al., 2015; Derry, 2015; Bowyer et al., 2020; Guilbaud et al., 2020).

These observations suggest that the mineralogy of Fe minerals formed under ferruginous water column conditions, and the precise diagenetic characteristics of the deposited sediments, play key roles in controlling concentrations of bioavailable P in the ocean. In addition to Fe (oxyhydr)oxide minerals such as ferrihydrite (Konhauser et al., 2007a), green rust (GR) is a prominent Fe mineral that may form in ferruginous settings, where it exerts an important control on nutrient cycling (Zegeye et al., 2012; Koeksoy et al., 2019). Green rust is a mixed Fe(II)/Fe(III) hydroxide, with brucite-like Fe(II)/Fe(III) tri-octahedral hydroxide layers alternated with interlayer anions (mainly CO_3^{2-} , Cl^- or SO_4^{2-}). Dependent upon the nature of the interlayer anions, GR particles adopt either a hexagonal geometry for the sulfated species (GRSO_4), or a rhombohedral geometry for the carbonated and chlorinated species (GRCO_3 and GRCl , respectively; Bernal et al., 1959; Simon et al., 2003).

Green rust formation can involve both biotic and abiotic pathways. Microbial activity can lead to the formation of GR during partial Fe(II) oxidation by nitrate reducing bacteria (Pantke et al., 2012; Etique et al., 2014) or photoferrotophys (Kappler and Newman, 2004), or by the bioreduction of ferric species under anoxic conditions (e.g., Fredrickson et al., 1998; Ona-Nguema et al., 2001; 2004; Kukkadapu et al., 2004; Berthelin et al., 2006; O'Loughlin et al., 2007; Zegeye et al., 2007a, b; Jorand et al., 2013). In the absence of microbial activity, GR can form directly by partial oxidation of $\text{Fe}(\text{OH})_2$ (e.g., Schwertmann and Fechter, 1994; Refait et al., 1997, 1998; Randall et al., 2001), the partial reduction of ferrihydrite or lepidocrocite by non-sulfidic reducing agents (Hansen, 1989), or by reaction between ferric (oxyhydr)oxides and Fe^{2+} (Usman et al., 2012). Green rust particles are metastable and tend to transform rapidly into more stable phases such as magnetite (e.g., Sumoondur et al., 2008; Guilbaud et al., 2013; Li et al., 2017; Halevy et al., 2017) and siderite (e.g., Benali et al., 2001; Halevy et al., 2017). However, the presence of P may stabilise GR minerals against transformation (Bocher et al., 2004; Barthélémy et al., 2012), whereby large amounts of P can adsorb at the lateral {010} and {100} surface sites, preventing GR oxidation and subsequent transformation into magnetite (Bocher et al., 2004; Ruby et al., 2006). Phosphorus can also incorporate into GR as interlayer anions during the partial reduction of P-doped ferrihydrite (Hansen and Poulsen, 1999). Hence, GR particles likely constitute an important sink for P under ferruginous water column conditions (Guilbaud et al., 2020).

The potential significance of vivianite (an Fe(II) phosphate ($\text{Fe}_3(\text{PO}_4)_2 \cdot 8\text{H}_2\text{O}$), arranged in monoclinic prismatic crystals; Nriagu, 1984; Mori and Ito, 1950) formation under ferruginous water column conditions is less clear. Using chemical equilibrium modelling, Derry (2015) suggested that vivianite formation in a ferruginous water column could have buffered the dissolved P concentration of mid-Proterozoic (1.8–0.8 billion years ago) oceans. In the modern day, water column vivianite formation is observed in the phosphate-rich ferruginous waters of Lake Pavin, where phosphate concentrations reach up to 300 μM at

the redoxcline (Cosmidis et al., 2014). However, under oligotrophic water column conditions, such as ferruginous Lake Matano (Crowe et al., 2008), vivianite is not observed, and instead GR is the dominant Fe mineral phase that forms in the water column (Zegeye et al., 2012). Moreover, whilst P adsorption is shown to stabilise GR against transformation (Bocher et al., 2004; Barthélémy et al., 2012), exposure of green rust to dissolved P is shown to promote GR transformation to vivianite (Hansen and Poulsen, 1999; Kukkadapu et al., 2004). This apparent contradiction suggests that the precise P concentration under ferruginous conditions may determine the mineralogy of authigenic Fe phases, which subsequently exerts a feedback control on the ultimate mobility and fate of P.

Within a euxinic water column, hydrogen sulfide promotes the dissolution of Fe (oxyhydr)oxides and subsequent precipitation of iron sulfides, which are significantly less efficient at adsorbing or coprecipitating P (Krom and Berner, 1980; 1981). As mentioned above, both the reductive dissolution of P-loaded Fe (oxyhydr)oxides and remineralisation of organic matter during microbial reduction constitute an effective source of dissolved P to porewaters, where it is potentially available to flux into the water column (e.g., Ingall and Jahnke, 1997; Slomp et al., 2004; Van Cappellen and Ingall, 1994). This may result in a positive feedback on primary production, hence increasing the flux of organic carbon to the sediment (e.g., März et al., 2008; Guilbaud et al., 2020; Alcott et al., 2022). Under euxinic conditions, re-adsorption of bioavailable P onto Mn or Fe (oxyhydr)oxides tends to occur only at the redoxcline (Turnewitsch and Pohl, 2010; Dijkstra et al., 2016, 2018), which results in limited P withdrawal from solution, compared to more efficient P scavenging under ferruginous conditions. However, modern sediment studies show that vivianite may form extensively in sediments deposited under euxinic conditions, at the interface where sulfide has been consumed and where Fe(II) released from the continued reduction of Fe (oxyhydr)oxides reacts with dissolved phosphate (e.g., Slomp et al., 2013; Hsu et al., 2014; Egger et al., 2015; Xiong et al., 2019).

The above considerations suggest that in low-P ferruginous environments, freshly formed GR particles may exert a primary control on the P cycle (Halevy et al., 2017), whereas under ferruginous conditions with higher phosphate (including in some sediment porewaters beneath a euxinic water column), the formation of vivianite may be the primary control. However, the specific control that P concentration exerts on the formation of Fe minerals has not been determined. Here we provide new experimental insight into the effect of P concentration on the formation of GR versus vivianite under anoxic conditions. We explore the effect of a changing P to Fe(II) ratio (from 1:150 to 1:3) on the precipitation of green rust versus vivianite, to determine potential thresholds for mineralogical changes. In addition, we test the effect of varying Fe(III) to Fe(II) ratios under conditions that deviate from the stoichiometry of green rust. These results provide new insight into controls on P cycling in modern and ancient anoxic settings.

2. Methods

2.1. Reagents

Experiments were conducted under CO_2 and O_2 -free conditions (<1 ppmv O_2), under a 98% N_2 and 2% H_2 atmosphere. H_2 was used to react with possible traces of O_2 on palladium catalysts. All solutions were prepared using 18.2 M Ω cm deionised water (MQ), purged with O_2 -free grade N_2 for 30 mins (Butler et al., 1994), and all salts were of analytical grade.

For the first set of experiments, we considered Fe(III) to Fe(II) ratios equivalent to stoichiometric green rust, across a range of P concentrations. An iron solution ('solution 1') was prepared by the dissolution of $\text{NH}_4\text{Fe}(\text{III})(\text{SO}_4)_2 \cdot 12\text{H}_2\text{O}$ and $(\text{NH}_4)_2\text{Fe}(\text{II})(\text{SO}_4)_2 \cdot 6\text{H}_2\text{O}$ to a final concentration of 6 mM Fe(III) and 12 mM Fe(II). Solution 1 was therefore the source of Fe(II), Fe(III) and sulfate ions required for the formation of GRSO_4 , with an Fe(III) to Fe(II) ratio of 1:2, equivalent to the

Table 1
Summary of experimental starting conditions and final solid crystalline products.

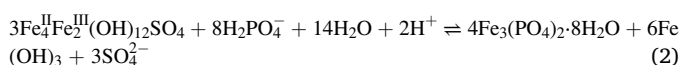
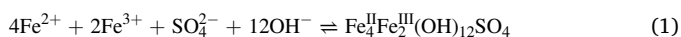
Exp	Solution mixing	Total Fe (mM)	Total P (mM)	NaOH (mM)	Fe(III):Fe(II)	P:Fe(II)	Observed crystallites
Exp 1	25 mL solution 1 + 25 mL solution 2	9	0	18	1:2	0	Green rust
Exp 2	25 mL solution 1 + 25 mL solution 2	9	0.08	18	1:2	1:150	Green rust
Exp 3	25 mL solution 1 + 25 mL solution 2	9	0.4	18	1:2	1:30	Green rust
Exp 4	25 mL solution 1 + 25 mL solution 2	9	2	18	1:2	1:6	Green rust + vivianite
Exp 5	25 mL solution 1 + 25 mL solution 2	9	4	18	1:2	1:3	Green rust + vivianite
Exp 6	25 mL solution 1 + 25 mL solution 2	9	8	18	1:2	2:3	Vivianite
Exp 7	25 mL solution 3 + 25 mL solution 5	9	0.45	18	1:8	1:17	Amorphous phases
Exp 8	25 mL solution 3 + 25 mL solution 6	9	0.2	18	1:8	1:36	Amorphous phases
Exp 9	25 mL solution 4 + 25 mL solution 5	9	0.45	18	1:4	1:17	Vivianite
Exp 10	25 mL solution 4 + 25 mL solution 6	9	0.2	18	1:4	1:36	Vivianite

stoichiometry of GRSO₄ (Ruby et al., 2003). Additionally, alkaline, phosphorus-bearing solutions ('solution 2') were prepared by the dissolution of NaOH (36 mM) and NaH₂PO₄ in various concentrations (ranging from 0 mM to 8 mM), where Exp 1 = 0 mM P, Exp 2 = 0.08 mM P, Exp 3 = 0.4 mM P, Exp 4 = 2 mM P, Exp 5 = 4 mM P, and Exp 6 = 8 mM P. Solution 2 provided the hydroxide source for the precipitation of GRSO₄, but also the phosphate ions for the co-precipitation of P with GR and/or the precipitation of Fe phosphate. The initial pH was 7.6–7.7 upon mixing the two solutions.

Additionally, we tested the effects of varying Fe(III), Fe(II) and P concentrations. For these experiments, we prepared two Fe solutions: 'solution 3', containing 2 mM Fe(III) and 16 mM Fe(II) (i.e., an Fe(III) to Fe(II) ratio of 1:8) and 'solution 4' containing 3.6 mM Fe(III) and 14.4 mM Fe(II) (i.e., an Fe(III) to Fe(II) ratio of 1:4). We further prepared a 0.9 mM P solution ('solution 5') and a 0.4 mM P solution ('solution 6') in 36 mM NaOH, in a similar manner to the first set of experiments. In all experiments, carbonate and silica were not included, in order to avoid the precipitation of siderite or greenalite.

2.2. Precipitation and ageing of Fe-P minerals under different P to Fe(II) ratios

Our aim was to explore the behaviour of P during the formation of GR (eq. (1); Ruby et al., 2003), as well as the competition between GR and vivianite formation under different P concentrations (eq. (2); modified after Hansen and Poulsen, 1999):



Six sets of experiments, defined based on the starting P concentrations of solution 2 outlined above, were conducted in serum bottles. For each set, 25 mL of solution 1 was titrated with 25 mL of solution 2 at a rate of 0.5 mL/s. This process was repeated several times for each experiment to conduct time series evaluations, whereby experiments were stopped and analysed after 0.25, 1, 2, 4, 8 and 24 h. When the two solutions were mixed, a dark-green precipitate appeared immediately. The serum bottles were sealed and taken outside the anoxic chamber to shake at 100 r/min. After the desired reaction time, the samples were re-introduced into the anoxic chamber for further preparation. At this point the pH of the slurry was measured using a HI 9024 pH meter. Then, a 10 mL aliquot of the slurry was taken and filtered on a PES filter (pore size

= 0.2 μm) to collect the filtrate for analysis of dissolved Fe(II), Fe(III) and P. Another 10 mL aliquot of the slurry was vacuum-filtered on a cellulose nitrate filter (pore size = 0.2 μm) in order to collect the solid phase. The solid samples were washed with MQ water, MgCl₂ and then a final MQ rinse to extract operationally defined 'loosely-bound' P, Fe(II) and Fe(III) fractions (Ruttenberg, 1992). The remaining 30 mL of the slurry was also vacuum filtered in the same way for XRD analysis. The collected solid phase was washed with 0.1 M NaCl and MQ to decrease the conductivity (Rothe et al., 2014), then mixed with 100 μL of glycerol to prevent oxidation during XRD analysis (Hansen, 1989; Guilbaud et al., 2013).

To complement these experiments, we tested the effect of a changing Fe(III) to Fe(II) ratio, departing from green rust stoichiometry. The aim here was to explore the mineralogical changes expected under conditions of active Fe(II) supply and lower Fe(III) to Fe(II) ratios. Four sets of experiments (Exp 7 to 10) were conducted, in which 25 mL of solution 3 or 4 was titrated with 25 mL of solution 5 or 6. Titration speed was set at a rate of 0.5 mL/s. The experiments were stopped and analysed after 24 h of aging, in the same manner as described above. All experimental starting conditions are summarised in Table 1.

2.3. Analytical procedures

Dissolved and loosely-bound Fe(II) concentrations were measured using a Genesys 6 spectrophotometer via the ferrozine method (Stookey, 1970; Viollier et al., 2000), with a relative standard deviation (RSD) of <2%. Dissolved and loosely-bound Fe(III) were reduced using 1.4 M hydroxylamine hydrochloride, and then measured via the same method. Dissolved and loosely-bound P concentrations were measured spectrophotometrically, via the molybdate blue method (Koroleff, 1976; Ruttenberg, 1992), with a RSD of <3%. Concentrations of Fe(II), Fe(III) and P in the solid phase were calculated by subtracting the dissolved and adsorbed pools from total (initial) concentrations.

Mineralogical analyses were performed on a Bruker AXS D8 diffractometer (Cu-Kα, voltage = 40 kV). Glycerol-coated samples were smeared on a silicon plate and sealed from the atmosphere in an air-tight dome inside the glovebox. Samples were analysed from 5 to 70° 2θ, with a step size of 0.05° 2θ and an integration time of 12 s.

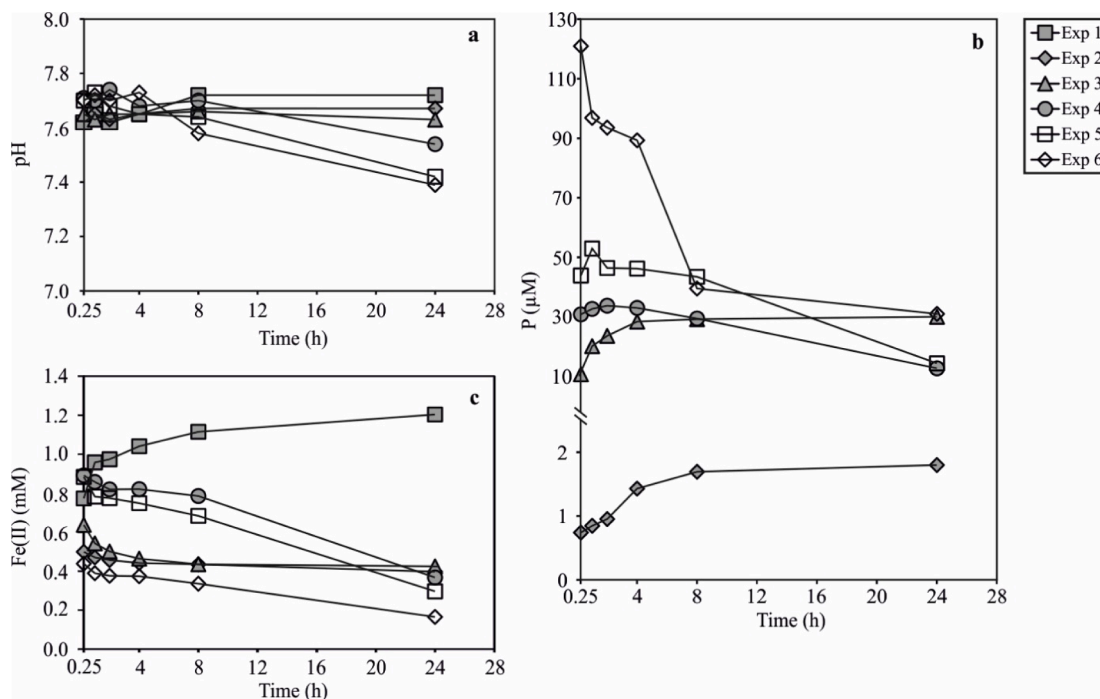


Fig. 1. Evolution of (a) pH, (b) dissolved P, and (c) dissolved Fe(II) through time, for all experiments. Note that Fe(III) was not detected in the dissolved phase. Error bars are within the size of the symbols.

3. Results

3.1. Experiments with constant Fe(III) to Fe(II) ratios

3.1.1. Dissolved species

For the first sets of experiments (Exp 1 to 6), the pH is relatively constant at 7.68 ± 0.04 during the first 4 h (Fig. 1a). For Exp 1–3, the pH remains fairly stable for the duration of the experiment. By contrast, for Exp 4–6, pH shows a decreasing trend after 8 h (although this decrease

starts earlier in Exp 6), and the extent of the decrease grows with increasing initial P concentration. Note that all experiments were conducted within the circumneutral to alkaline pH window where both GR and vivianite can form (e.g., Ruby et al., 2003; Madsen and Hansen, 2014).

The evolution of dissolved [P] through time is illustrated in Fig. 1b. For Exp 2 and 3, dissolved [P] increases dramatically within the first 4 h, from 0.74 to 1.43 μM and from 10.6 to 28.4 μM , respectively. After 4 h, the rate of dissolved [P] increase slows down, and from 8 to 24 h,

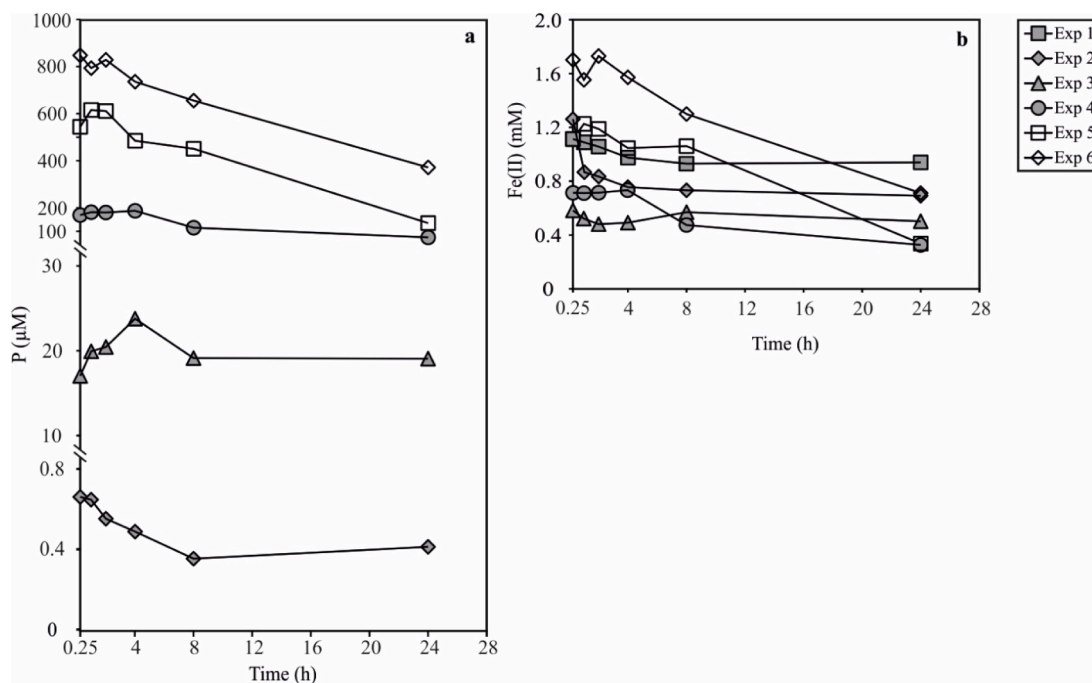


Fig. 2. Profiles of (a) loosely-bound P, and (b) loosely-bound Fe(II) through time, for all experiments. Note that Fe(III) was not detected as an adsorbed species. Error bars are within the size of the symbols.

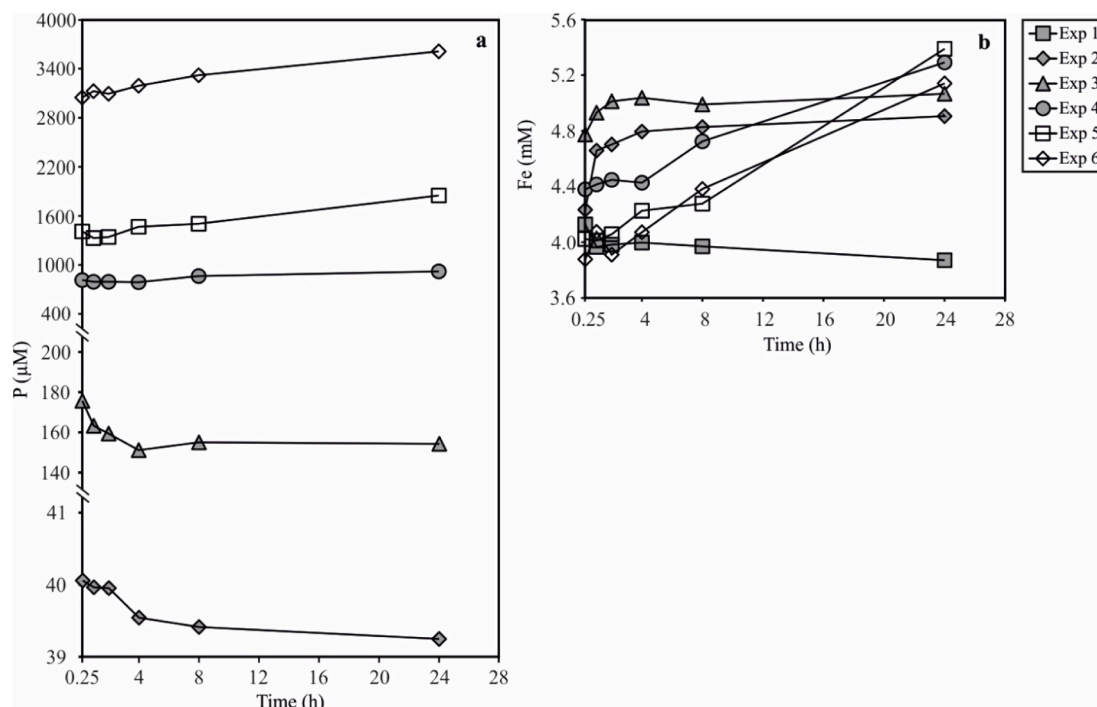


Fig. 3. Profiles of (a) solid P, and (b) solid Fe(II) through time, for all experiments. Error bars are within the size of the symbols.

dissolved [P] stabilises. For Exp 4 and 5, dissolved [P] increases in the first two hours and in the first hour, respectively, but then decreases to 12.7 and 14.3 μM , respectively. For Exp 6, dissolved [P] decreases throughout the experimental duration, but [P] decreases at slower rate after 8 h, to reach a concentration of 30.9 μM after 24 h.

Dissolved [Fe(II)] is shown in Fig. 1c. Note that dissolved Fe(III) was below detection ($<1.5 \mu\text{M}$) throughout all experiments, and thus dissolved Fe exclusively comprised ferrous iron. In the absence of P (Exp 1), dissolved [Fe(II)] increases with time, from 0.77 to 1.20 mM. For the other five experiments, dissolved [Fe(II)] decreases throughout the experimental duration. Exp 2 and 3 show similar dissolved Fe(II) profiles, with a sharper decrease within the first 4 h, from 0.50 to 0.44 mM and from 0.64 to 0.46 mM, respectively, followed by a smoother decrease until 24 h. Exp 4 and 5 also show similar dissolved Fe(II) profiles, with a smoother decrease within the first 4 h and first 2 h, respectively, and then dissolved Fe(II) decreases progressively more sharply, to reach 0.37 and 0.30 mM, respectively, after 24 h. For Exp 6, dissolved [Fe(II)] decreases from 0.44 mM at 15 min to 0.17 mM after 24 h, with stable concentrations ($0.38 \pm 0.01 \text{ mM}$) between 1 h and 4 h.

3.1.2. Loosely-bound P, Fe(II) and Fe(III) species

MgCl_2 -extractable P profiles were measured for the five experiments containing P (Fig. 2a). For Exp 2, loosely-bound P decreases from 0.66 to 0.35 μM in the first 8 h, then remains stable at $0.38 \pm 0.03 \mu\text{M}$ from 8 to 24 h. For Exp 3–5, there is a clear increase in loosely-bound P, from 17.0 to 23.8 μM , from 169.2 to 187.4 μM , and from 544.0 to 615.7 μM , respectively, followed by a strong decrease in loosely-bound P. After 8 h, adsorbed P remains constant at $19.10 \pm 0.03 \mu\text{M}$ for Exp 3, whereas loosely-bound P continues to decrease for the other experiments. We also note that the decrease in loosely-bound P starts earlier for Exp 5. For Exp 6, loosely-bound P decreases rapidly throughout the experimental duration.

Both loosely-bound Fe(II) and Fe(III) were measured in the 6 experiments from 15 mins to 24 h (Fig. 2b). Loosely-bound Fe(III) was not detected. For Exp 1 and 2, loosely-bound Fe(II) decreases in the first 8 h, and remains constant from 8 to 24 h, at 0.93 ± 0.01 and 0.71 ± 0.02 mM, respectively. For Exp 3, loosely-bound Fe(II) decreases slightly

from 0.58 to 0.48 mM in the first 2 h, then increases slightly from 2 to 8 h, followed by a slight decrease from 0.57 to 0.50 mM from 8 to 24 h. For Exp 4, loosely-bound Fe(II) stays constant at $0.72 \pm 0.02 \text{ mM}$ in the first 4 h, followed by a rapid decrease from 0.74 to 0.33 mM from 4 to 24 h. For Exp 5 and 6, loosely-bound Fe(II) remains relatively constant for the first 2 h, at 1.18 ± 0.07 and $1.66 \pm 0.11 \text{ mM}$, respectively. However, from 2 to 24 h, loosely-bound Fe(II) decreases rapidly from 1.19 to 0.34 mM and from 1.73 to 0.71 mM, respectively.

3.1.3. P, Fe(II) and Fe(III) in solid phase

P profiles in the solid phase essentially mirror the trends observed for dissolved species (Fig. 3a). For Exp 2 and 3, solid phase P decreases dramatically over the first 4 h. After 4 h, the rate of solid phase P decrease slows down in Exp 2, but in Exp 3, solid phase P increases slightly from 4 to 8 h, subsequently remaining stable. For Exp 4 and 5, solid phase P decreases within the first 4 h and 1 h, respectively, but then increases to 921.4 and 1848.7 μM , respectively. For Exp 6, solid phase P increases throughout most of the experimental duration, but the rate of solid phase P increase slows down after 8 h.

Fe(II) profiles in the solid phase also mirror the trends observed in dissolved Fe(II) (Fig. 3b). In the absence of P (Exp 1), solid phase Fe(II) shows an overall decreasing trend with time, from 4.13 to 3.87 mM, but in the other five experiments, solid Fe(II) shows an overall increasing trend. Exp 2 and 3 have similar profiles, where solid Fe(II) increases dramatically within the first hour, followed by a constant increase until 24 h. Exp 4 and 5 also show similar solid Fe(II) profiles, with a smoother increase within the first 4 h and first 2 h, respectively, followed by a rapid increase until 24 h. For Exp 6, solid Fe(II) shows an overall increasing trend with time, from 3.88 to 5.14 mM. Since no adsorbed or dissolved Fe(III) are detected in any experiment, and there is no electron donor to reduce Fe(III), solid mineral Fe(III) effectively accounts for 100% of the total dissolved Fe(III) added.

3.1.4. Mineralogy of the solid phase

The mineralogical evolution of the samples was analysed after 15 min, 4 h, 8 h and 24 h for the six experiments. For Exp 1–3 (i.e., in the absence of P, or with low initial P concentrations), GR is the only

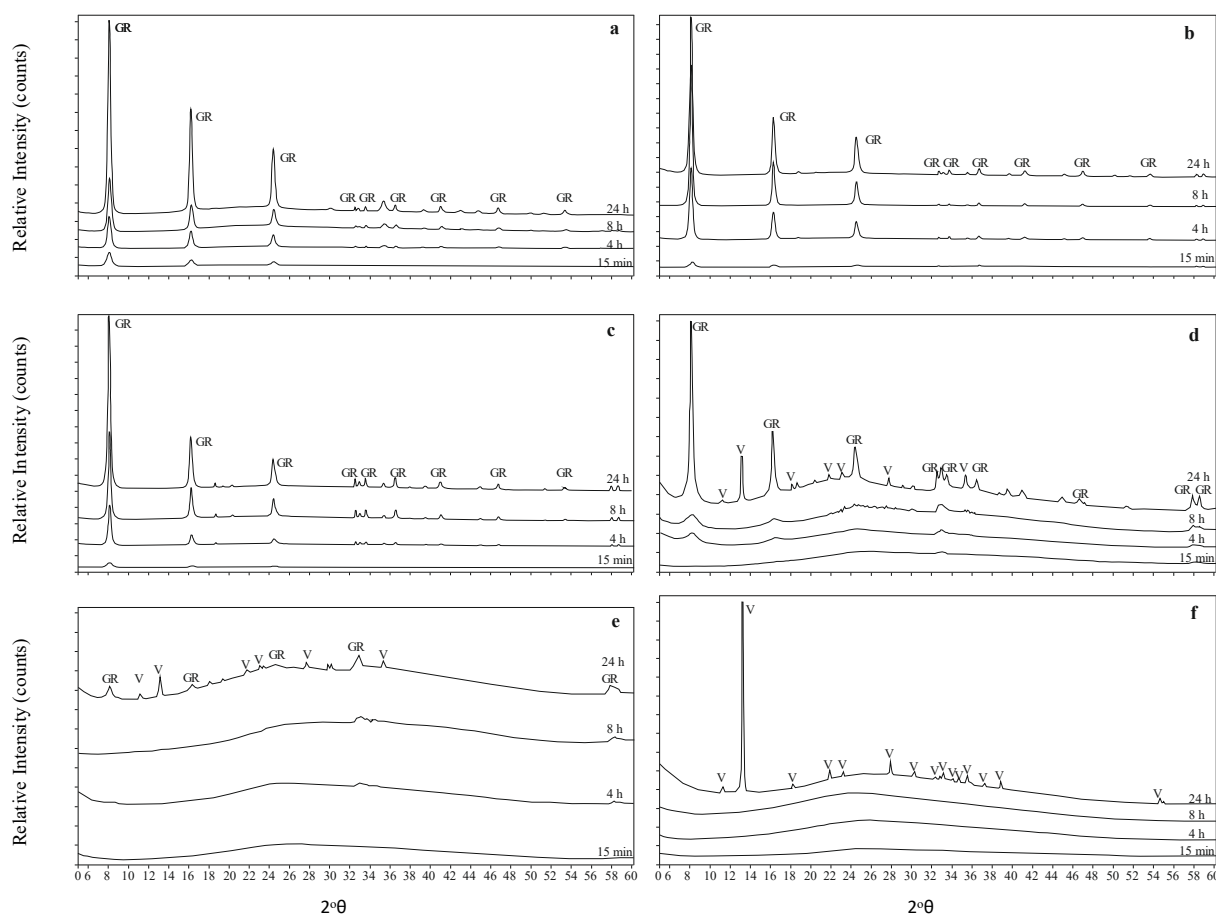


Fig. 4. XRD spectra of the collected solids, for Exp 1 to 6 (a to f). ‘GR’ represents green rust and ‘V’ represents vivianite.

Table 2

Details of dissolved, loosely-bound, solid and total P and Fe (II) in experiments with varying Fe(III) to Fe(II), after 24 h of ageing.

Group	Dissolved P (μM)	Dissolved Fe (II) (mM)	Adsorbed P (μM)	Adsorbed Fe (II) (mM)	Solid P (μM)	Solid Fe (II) (mM)	Total P (μM)	Total Fe (II) (mM)	Total Fe (III) (mM)
Exp 7	0.57	1.30	32.55	0.15	416.87	6.55	450	8	1
Exp 8	0.52	1.19	12.41	0.10	187.08	6.71	200	8	1
Exp 9	2.34	0.84	30.06	0.12	417.60	6.24	450	7.2	1.8
Exp 10	4.98	0.99	9.92	0.14	185.10	6.08	200	7.2	1.8

mineral identified throughout the experiment (Fig. 4a, b and c). Furthermore, XRD peak intensities increase with time, indicating that GR particles become progressively more crystalline. For Exp 4, the first 15 min of experiment are characterized by an absence of identifiable peaks, which start developing after 4 h (Fig. 4d). At 24 h, both GR and vivianite peaks are identified. For Exp 5, the delay in peak development is even more severe, with the first identifiable peaks restricted to the 24 h experiment (Fig. 4e). A delay in peak development also occurs in Exp 6, but the 24 h experiment shows well developed vivianite peaks (Fig. 4f), with no crystalline GR phase detected. We note that while no crystalline minerals other than GR and vivianite are detected, this does not rule out the possible formation of amorphous P-, Fe(II)- and Fe(III)-bearing phases.

3.2. Experiments with variable Fe(III) to Fe(II) ratios

Final dissolved, loosely-bound and solid concentrations of Fe(II) and P for Exp 7 to 10 are summarised in Table 2. After 24 h of ageing, the majority of the P and Fe precipitates out of solution as a solid phase, or to

a lesser extent, as loosely-bound species, in agreement with the previous set of experiments. At lower Fe(III) to Fe(II) ratios (Exp 7 and 8), initial P and Fe concentrations have no substantial effect on subsequent dissolved P and Fe concentrations, which cluster around 0.55 μM and 1.25 mM, respectively. At higher Fe(III) to Fe(II) ratios (Exp 9 and 10), the final dissolved P concentrations are inversely proportional to initial P concentrations (i.e., experiments involving higher P contents enhance P trapping in the solid phase).

Mineralogical analyses of the solid precipitates for experiments 7 to 10 (Fig. 5) suggest that vivianite is the only crystalline phase present after 24 h of ageing. At lower Fe(III) to Fe(II) ratios (Exp 7 and 8), however, no crystallite is detected. At higher Fe(III) to Fe(II) ratios (Exp 9 and 10), diffraction peaks for vivianite are more pronounced for Exp 9 (Fig. 5c), suggesting that higher P promotes the development of more crystalline vivianite.

4. Discussion

The ratios of P to Fe(II) chosen in this study cover the range of P:Fe

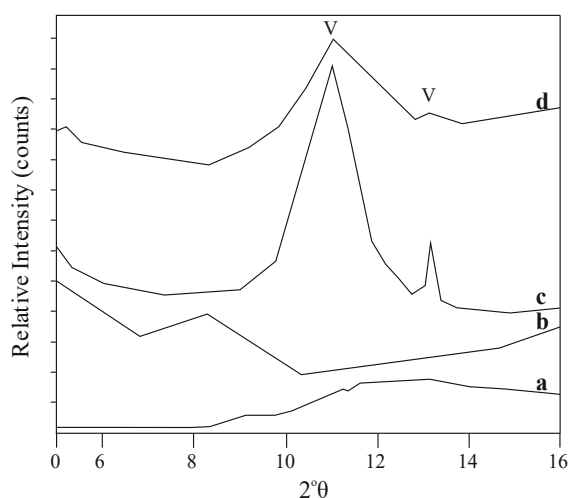


Fig. 5. XRD spectra of collected solids after 24 h of aging, for Exp 7 to 10 (a to d on the figure). ‘V’ = vivianite.

Table 3

Phosphorus to iron ratios and the nature of authigenic and highly reactive, non-sulfidic, Fe(II) minerals in a range of stratified lakes.

Lake Name (reference)	Location of the geochemical/mineralogical analysis	P:Fe(II) ratio	Authigenic Fe(II)-bearing non-sulfidic minerals
Lake Matano (Crowe 2008; Zegeye et al., 2012)	Water column, at 118 m depth	< 1:30	Green rust
Lake Matano (Crowe 2008; Bauer et al., 2020)	Anoxic sediments	Unknown	Magnetite
Lake Towuti (Bauer et al., 2020; Vuillemin et al., 2020)	Water column directly above the sediment	< 1:500	Green rust
Lake Towuti (Vuillemin et al., 2019)	Anoxic sediments	Between 1:150 and 1:2700	Siderite
Lake Pavin (Busigny et al., 2014; Cosmidis et al., 2014)	Water column, at 67 m depth	1:6	Vivianite
Lake Pavin (Busigny et al., 2014; Cosmidis et al., 2014)	Water column, at 86 m depth	1:3	Vivianite
Lake Cadagno (Xiong et al., 2019)	Sulfide-depleted anoxic sediments	1:1.3 to 1:2	Vivianite

(II) ratios found in many modern water bodies and porewaters (Table 3). For example, Exp 1, Exp 2 and Exp 3 (with P:Fe(II) ratios of 0, 1:150 and 1:30, respectively) correspond to the range in ratios observed in the oligotrophic ferruginous waters of Lake Towuti (Vuillemin et al., 2020) and Lake Matano (Crowe, 2008; Crowe et al., 2008; Zegeye et al., 2012). In Exp 4 and Exp 5, P:Fe(II) ratios were 1:6 and 1:3, respectively, which are similar to ratios found in the water column of the anoxic ferruginous Lake Pavin (Busigny et al., 2014). In Exp 6, the P:Fe(II) ratio corresponds to the sulfide-depleted porewaters of the euxinic Lake Cadagno (Xiong et al., 2019).

4.1. Green rust formation

The pH profiles described above suggest mineral precipitation and transformation throughout the experiments. As indicated by the XRD patterns for the P-free experiment (Exp 1), GR was the sole mineral detected, and its mechanism of formation appears to be constant throughout the experiment, as indicated by a relatively stable pH of 7.64 ± 0.02 (see also Ruby et al., 2003; Guilbaud et al., 2013). Unlike previous reports (Guilbaud et al., 2013), however, we do not observe a rapid transformation of GR to more stable magnetite, and crystalline magnetite remains absent from the diffractograms even at 24 h. This is likely due to the higher reactant concentrations (including NaOH) used in the Guilbaud et al. (2013) experiments, which may trigger a more rapid transformation to magnetite at higher pH. However, we did observe a slight increase in pH after 4 h, which might indicate very minor formation (below detection by XRD) of magnetite (Fig. 4a). Yet, the observed increase in dissolved Fe(II) concentrations in the P-free experiment reflects loss of Fe(II) from the solid phase, which is inconsistent with magnetite formation during transformation from GR (Sumoondur et al., 2008; Guilbaud et al., 2013). Hence, the increase in both pH and dissolved Fe(II) most likely reflects phase equilibration during crystal growth by Ostwald ripening (Guilbaud et al., 2013), and thus the dominant operating reaction can be summarized by eq. (1).

In fact, the pH stability (7.69 ± 0.05) observed during the first 4 h of all other experiments where P is present (Exp 2 to 6), suggests that the system might be more generally controlled by GR formation upon P addition throughout these early stages, at any P concentration. Indeed, the presence of GR peaks on the XRD diffractograms for Exp 2–5 (Fig. 4b, c, d and e) confirms GR precipitation. However, the earlier stages for experiments performed at higher P concentrations (Exp 4–6) are characterized by an absence of GR peaks (Fig. 4d, e and f), which we discuss in more detail below.

4.2. Coupled Fe and P cycling at low P concentrations

At low P concentrations (Exp 2 and 3), the early experimental stages (0–4 h) are characterized by a decrease in dissolved Fe(II) (Fig. 1c), with a concomitant increase in solid-phase Fe(II) (Fig. 3b). We also observe a synchronous increase in dissolved P and decrease in solid-phase P (Fig. 1b and 3a), which suggests that dissolved P is sourced from the solid phase. Bocher et al. (2004) showed that P efficiently adsorbs to the lateral faces of GRCO_3 particles, rather than being incorporated into the interlayers of the mineral, implying that the increased dissolved P concentrations originate through surface desorption, rather than release of interlayer phosphate anions. However, the geometry of GRCO_3 is fundamentally different to the geometry of GRSO_4 , which may, by contrast, exchange interlayer sulfate with phosphate (Hansen and Poulsen, 1999). Furthermore, at $\text{pH} < 7.8$, the surface chemistry of GRCO_3 is largely dominated by positively charged Fe_3OH_2^+ sites, with a site concentration of $>0.45 \text{ mmol.g}^{-1}$ (Guilbaud et al., 2013). Assuming a similar surface chemistry for GRSO_4 , this would imply unsaturated sites in our experiment, with the potential to adsorb more P. Hence, our experimental conditions suggest that during these early stages, surface sites constitute a sink for phosphate anions (as adsorbed P), rather than a source for dissolved P. Therefore, we conclude that the initial increase in dissolved P reflects release from trapped interlayer phosphate during crystal growth.

4.3. Vivianite formation at higher P concentrations

At higher [P] (Exp 4–6), the pronounced decrease in pH suggests an alternative reaction to eq. (1). XRD patterns reveal the precipitation of a secondary phase consisting of vivianite (Fig. 4d and e), suggesting that at higher [P], dissolution of GR and subsequent precipitation of vivianite occurs (eq. (2)). This is also supported by a continuous dissolved P decrease after the first hour of the experiment (Fig. 1b), which is

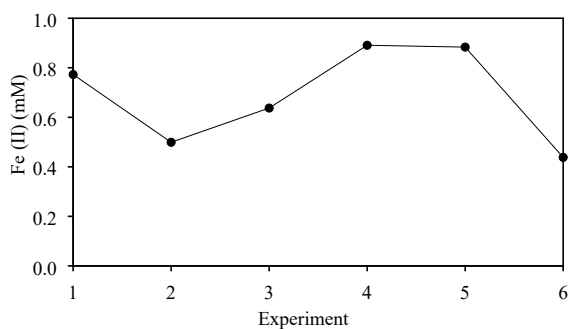


Fig. 6. Dissolved Fe(II) concentrations in solution after 15 mins of reaction in the 6 different experiments. Error bars are within the size of the symbols.

accompanied by a concomitant decrease in loosely-bound P and increase in solid-phase P (Fig. 3a). Similar trends are observed for dissolved and solid-phase Fe, which both support the precipitation of secondary Fe-P minerals, in agreement with the observed change in pH.

In Exp 6, which is characterized by the highest [P], there is no observable P increase during the initial stages, and instead, dissolved P decreases from the start of the experiment (Fig. 1b), while solid-phase P increases rapidly (Fig. 3a). We note that the evolution of dissolved species does not stabilise after 24 h, which implies that the system had

not reached chemical equilibrium. The observed Fe-P dynamics suggest that dissolved P precipitates as amorphous Fe-P precursors, perhaps without the intervention of intermediate GR minerals. This appears to be supported by the mineralogical data (Fig. 4f), which show that vivianite, rather than GR, constitutes the only measurable crystallite in the system. Since dissolved Fe(III) is not detected during the experiment, it is reasonable to state that the solid amorphous precursors are likely to include ferric species such as $\text{Fe}(\text{OH})_3$, whose precipitation is favoured between pH 7 and 8 (Christian, 2014), and which are known to be very efficient scavengers of dissolved P.

4.4. A mechanism for P uptake by green rust and vivianite

The delay in the development of crystalline phases when phosphate is present has been reported for a range of ferric (oxyhydr)oxide minerals (Gálvez et al., 1999) and GR (Hansen and Poulsen, 1999). In all cases, the first precipitates include either poorly crystalline or amorphous ‘greenish’ P-Fe phases, prior to the development of crystalline species (Hansen and Poulsen, 1999). Mechanistically, GR formation is preceded by the precipitation of a ferric (oxyhydr)oxide, followed by the substitution of OH^- by SO_4^{2-} at the FeOOH surface and formation of an $\text{Fe}(\text{OH})_2$ brucite-like cluster which nucleates GR (see Ruby et al., 2006). In the absence of phosphate, this occurs within milliseconds, and is not observable by our experimental set-up.

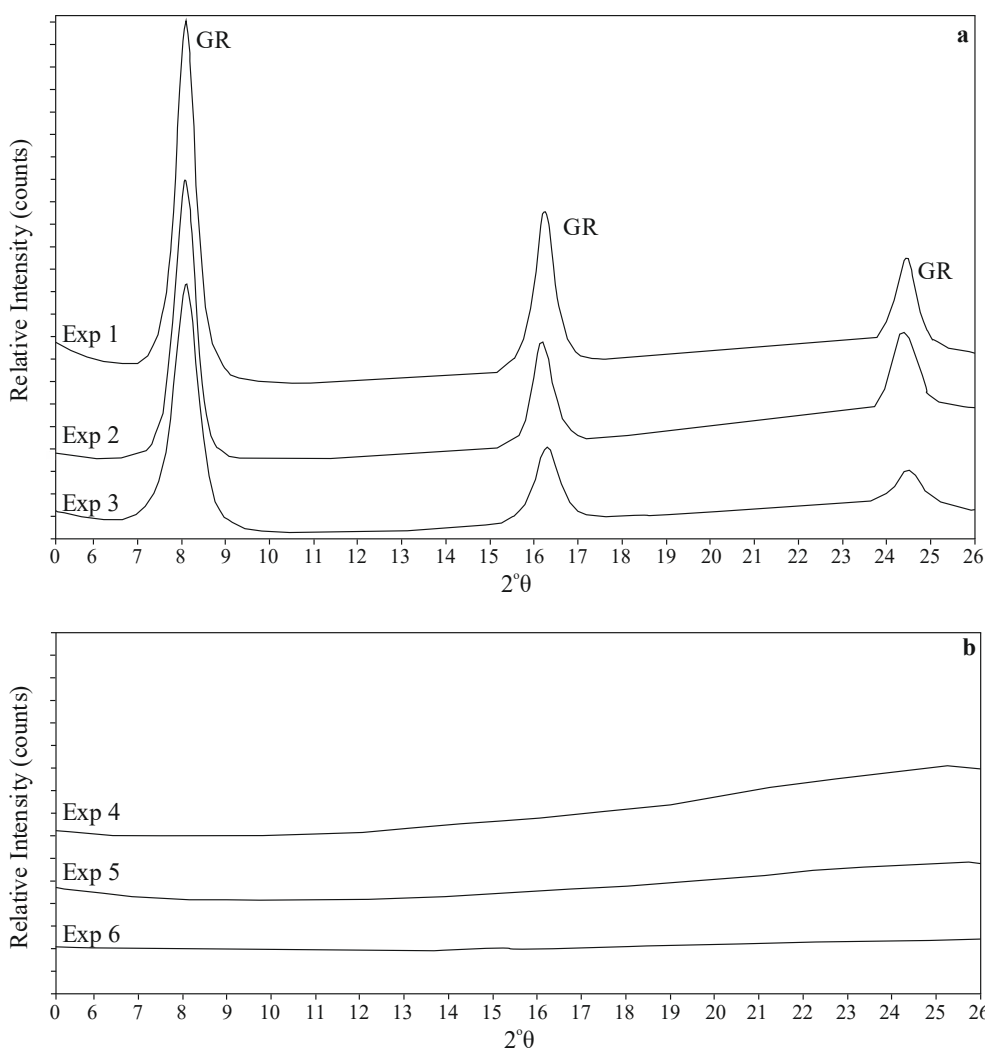


Fig. 7. XRD spectra of the collected solids for the 15 min reaction. ‘GR’ represents green rust. For Exp 1–3 (a), the data are consistent with crystalline GR, whereas for Exp 4–6 (b), no detectable crystallite is observed.

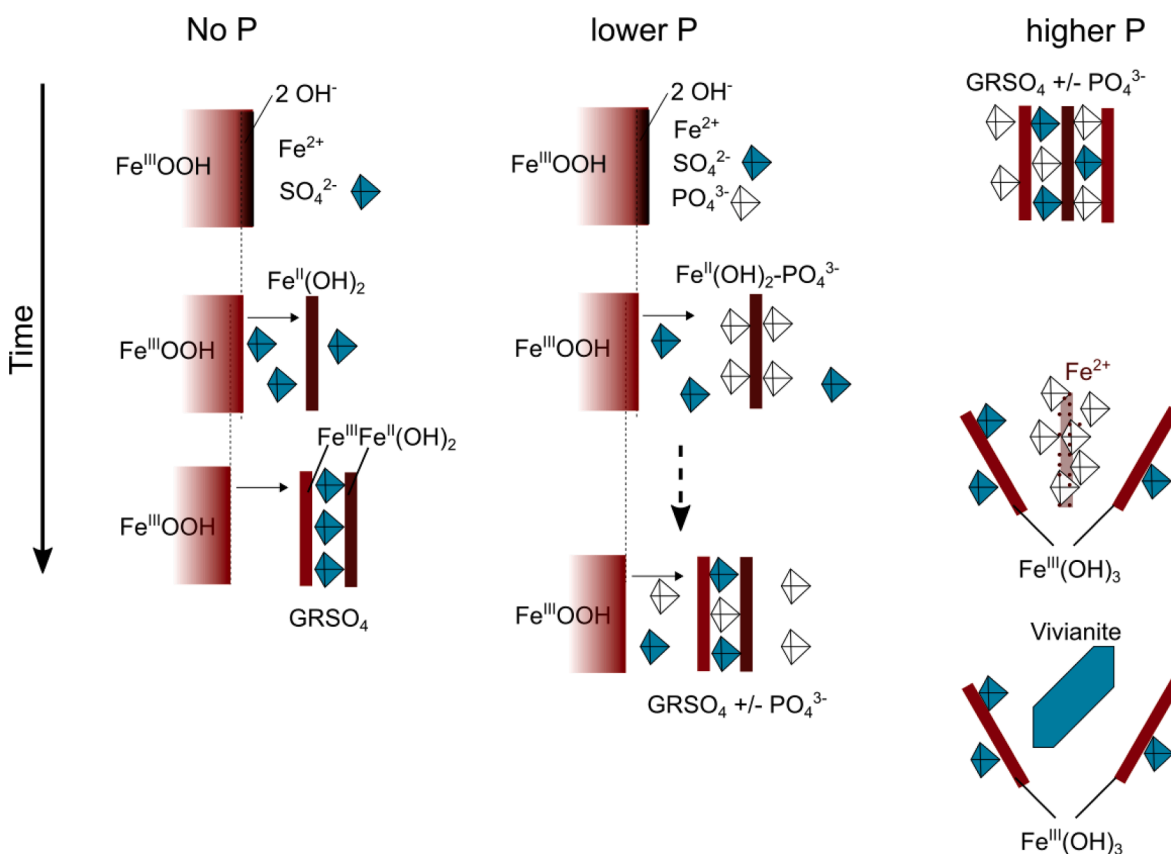


Fig. 8. Sketch representing the mechanism of green rust versus vivianite formation through time, with varying P concentrations. On the left-hand panel, no P is present and GR rapidly crystallises (via an FeOOH precursor, while Fe^{2+} and sulfate, represented by the blue tetrahedra, remain in solution). With low P concentrations ($\text{P}:\text{Fe} < 1:30$, middle panel), phosphate (represented by the white tetrahedra) associates with neo-formed $\text{Fe}(\text{OH})_2$ clusters, delaying the crystallisation of GR, which eventually forms and incorporates phosphate as interlayer anions. With higher P concentrations ($\text{P}:\text{Fe} > 1:30$, right-hand panel), GR starts to dissolve, releasing $\text{Fe}(\text{II})_{\text{aq}}$ and phosphate from its interlayers, which react to form vivianite.

Comparing the dissolved Fe(II) concentrations at 15 min when P is present (Figs. 6 and 7) gives insight into the mechanism responsible for the delay in crystallite formation. The drop in dissolved $[\text{Fe}(\text{II})]$ (from 0.77 to 0.50 mM, Fig. 6) for Exp 2, coupled with formation of less crystalline GR (Fig. 7a), reflects the rapid formation of an amorphous (i.e., not detected by XRD), P-bearing Fe phase. The nature of this phase (or assemblage of phases) is unknown, although it likely consists of phosphate-associated $\text{Fe}(\text{OH})_2$ clusters, delaying the early development of more crystalline GRSO_4 (Fig. 8). With time, these initial amorphous precipitates recrystallize into the more stable, P-bearing GRSO_4 , as shown by the XRD diffractograms (Fig. 4b; Fig. 8). For P concentrations > 2 mM (Exp 4 to 6), dissolved Fe(II) concentrations increase from 0.50 to 0.89 mM at 15 min (Fig. 6). This suggests that increasing P concentration promotes the release of Fe(II) during GR dissolution, which eventually converts to Fe(II) phosphate (eq. (2)), inhibiting the development of highly crystalline GR (Hansen and Poulsen, 1999; Fig. 7a and b; Fig. 8).

As P reaches its highest initial concentration, dissolved Fe(II) decreases to 0.44 mM (Fig. 6), implying that an alternative mineralization pathway operates under these conditions, with about half of dissolved Fe(II) (0.44:0.89) reacting directly with dissolved P without the intervention of GR. The formation of this amorphous (XRD-undetected) intermediate phase during the conversion of interlayered-phosphate GR to vivianite (Hansen and Poulsen, 1999) explains the lag time in vivianite crystallization, which occurs between 8 and 24 h (Figs. 7b and 9b). To assess why vivianite does not form more rapidly, we explore the evolution of the solid-phase molar Fe(II):P ratio during the course of Exp 6 (Fig. 10). It appears that from 15 min to 24 h, the ratio increases from 1.27 to 1.42, which is close to stoichiometric vivianite. This suggests

that early Fe-P precipitates carry an excess of P with respect to the stoichiometry of vivianite, favouring the precipitation of amorphous Fe(II) precursors which later develop into vivianite.

4.5. Fe-P dynamics under Fe(II)-rich conditions

Departing from Fe(III) to Fe(II) ratios that are stoichiometrically favourable for either GR or vivianite formation, we now explore the competitive role of both minerals in P cycling. Under our highest Fe(II) conditions (i.e., Exp 7 and 8), a stability phase diagram shows that GRSO_4 and amorphous $\text{Fe}(\text{OH})_2$ first precipitate in the proportions of 25% and 75%, respectively (see Ruby et al., 2006), and no XRD-detectable crystallites are observed after 24 h, independent of P content (Fig. 5). Under such mineralogical conditions, one can assume that the majority of P is trapped as $\text{Fe}(\text{OH})_2 \cdot \text{PO}_4$. When Fe(III) concentrations are higher (i.e., Exp 9 and 10), GRSO_4 and amorphous $\text{Fe}(\text{OH})_2$ precipitate in equal proportions (Ruby et al., 2006), resulting in a higher proportion of P being trapped as P-bearing GRSO_4 . After 24 h, the only XRD-detectable phase consists of vivianite, consistent with it being more crystalline at higher P contents.

These results, although coherent with Exp 1–6, might appear counter-intuitive, as vivianite is detected solely when Fe(III) contents increase. Hence, together with our previous set of experiments, our results strongly support a model where vivianite forms when Fe(III) is initially present, i.e., when a GR precursor (or an amorphous, P-bearing Fe(III)/Fe(II) equivalent) is involved. Because of the effectiveness of GR at scavenging P, such a precursor phase may act as a P-concentrating mineral, favouring the subsequent formation of crystalline vivianite when P concentrations are high enough. By contrast, under conditions

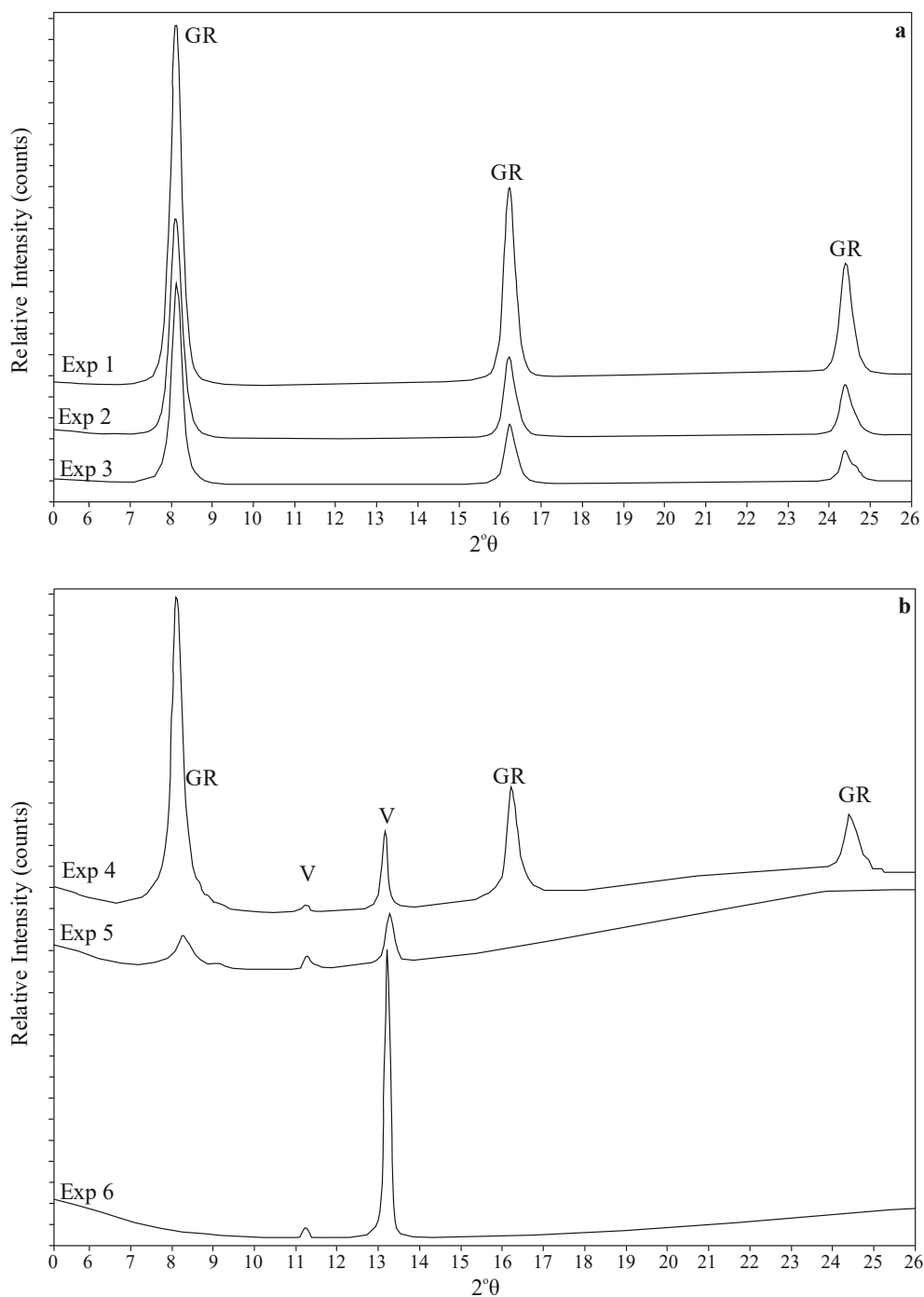


Fig. 9. XRD spectra of the collected solids after 24 h of reaction. ‘GR’ represents green rust and ‘V’ represents vivianite. Exp 1–3 (a) only comprise crystalline GR, whereas Exp 4–6 (b) comprise either a mix of GR and vivianite, or crystalline vivianite only.

where Fe(II) is abundant and $\text{Fe(II)} \gg \text{Fe(III)}$, P partitioning will occur between GR and Fe(OH)_2 , and vivianite formation depends on the prior accumulation of P by GR.

Together, our results reconcile both experimental and natural observations (Table 1). In settings such as Lake Matano and Lake Towuti, with dissolved $\text{P:Fe(II)} < 1:30$, P drawdown is effectively controlled by exchange with, and adsorption onto, GR species, via amorphous Fe-P precursor phases. Subsequently, since GR is relatively unstable, transformation to more stable minerals such as magnetite (Bauer et al., 2020) or siderite (Vuillemin et al., 2019) may occur during diagenesis, with the rate of these transformations potentially being slowed due to P stabilization of the GR. By contrast, under conditions where P is relatively

more abundant (i.e., dissolved $\text{P:Fe(II)} > 1:30$), such as in the water column of Lake Pavin or in the deeper porewaters of Lake Cadagno, formation of vivianite commonly occurs (Cosmidis et al., 2014; Xiong et al., 2019).

4.6. Implications for the redox cycling of P in ancient oceans

The particulate ‘Fe shuttle’ for delivery of P to the sediment is a popular hypothesis to invoke P-limited productivity in ancient ferruginous oceans (e.g., Bjerrum and Canfield, 2002; Laakso and Schrag, 2014; Jones et al., 2015; Derry, 2015; Reinhard et al., 2017; Guilbaud et al., 2020). The P record from banded iron formations is notoriously difficult

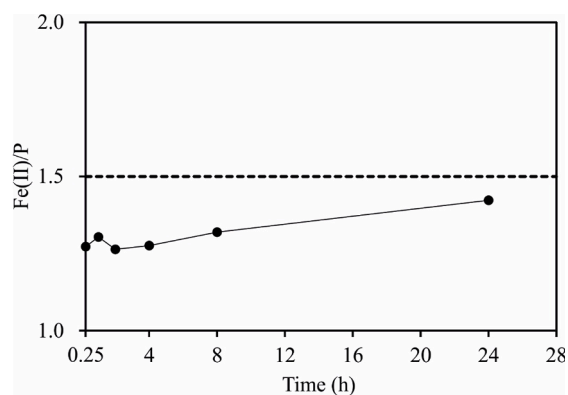


Fig. 10. Evolution of the molar Fe(II)/P ratio through time for Exp 6 ([P] = 8 mM). The dashed line represents stoichiometric vivianite.

to constrain, however, as experimental estimates for the distribution coefficient between dissolved P and P co-precipitated with ferrihydrite has led to conflicting results and interpretations of oceanic P levels, that are dependent on the precise experimental conditions that were employed (Bjerrum and Canfield, 2002; Konhauser et al., 2007a; Planavsky et al., 2010; Jones et al., 2015). Moreover, the potential dominant role of GR in controlling dissolved P concentrations (Guilbaud et al., 2013; Halevy et al., 2017; Guilbaud et al., 2020) is not considered in this earlier work. Although we did not perform our experiments under silica-rich, Precambrian-like seawater conditions, our results reinforce the potential role of GR as a control on dissolved P concentrations in ferruginous settings characterised by relatively low P:Fe(II) ratios. Such conditions occur in modern oligotrophic ferruginous settings such as Lake Matano and Lake Towuti (Crowe et al., 2008; Zegeye et al., 2012; Vuillemin et al., 2016), which are considered prime analogues for the ancient oligotrophic ferruginous oceans that were prevalent across huge swathes of Earth history, including in the earlier Archean (Canfield et al., 2006; Jones et al., 2015) and early Neoproterozoic (Guilbaud et al., 2020).

By contrast, Derry (2015) argue that vivianite formation, rather than GR, may have played a dominant role in scavenging dissolved Fe²⁺ from ferruginous Proterozoic oceans. However, the model of Derry (2015) focuses on the saturation state of vivianite with respect to dissolved Fe²⁺ and P concentrations in the ocean, without further consideration of Fe (III) species. As a result, rather low P:Fe(II) ratios (1:370 and 1:160 at pH 7.5 and pH 8, respectively) are implied to be sufficient to promote vivianite formation, which is not supported by our experimental results or observations of low-P ferruginous settings (Zegeye et al., 2012). Our study suggests, however, that vivianite formation may exert a major control on P cycling and bioavailability under higher P conditions. Such conditions have been shown to occur in modern eutrophic-mesotrophic ferruginous settings (Cosmidis et al., 2014; O'Connell et al., 2015; Kubeneck et al., 2021), as well as in euxinic settings where an excess of reactive Fe minerals over dissolved sulfate, coupled with depletion of sulfate during early diagenesis, promotes vivianite formation over pyrite formation (März et al., 2008; Slomp et al., 2013; Hsu et al., 2014; Egger et al., 2015; Xiong et al., 2019; Kubeneck et al., 2021). Both scenarios are likely to have prevailed at different times in Earth history, including at the redoxcline or during early diagenesis in late Archean and mid-Proterozoic euxinic continental margin settings (Cosmidis et al., 2014; Poulton, 2017; Guilbaud et al., 2020), as well as during episodes of low-sulfate ferruginous and euxinic ocean anoxia in the Phanerozoic (e.g., März et al., 2008).

5. Conclusions

This study shows that P concentration exerts a first order control on

the mineralogy of Fe minerals that may form under anoxic conditions. Pure GR_{SO4} readily forms in the absence of P, or at low P concentrations. For P:Fe(II) ratios <1:30, P extensively adsorbs at the surface of GR particles, and exchanges with sulfate in the interlayers. This results in GR minerals of poorer crystallinity, but which are also likely somewhat more resistant in terms of their rate of transformation into common secondary minerals, such as magnetite or siderite. Nevertheless, observations of modern low P settings, such as Lake Matano and Lake Towuti, suggest that at least part of the GR that forms in the water column (Zegeye et al., 2012) may ultimately transform to magnetite during diagenesis under such conditions (Vuillemin et al., 2019; 2020).

The ultimate behaviour of P during transformation of GR to secondary minerals during diagenesis is likely highly variable, however, and will undoubtedly be influenced by the depth in the sediment profile where such transformations occur, as well as the precise chemistry of the porewaters. Indeed, in settings where the concentration of P increases significantly during diagenesis, as may occur in many organic-rich sediments due to release of P during organic matter remineralisation coupled with the reductive dissolution of Fe (oxyhydr)oxide minerals, GR will begin to dissolve, allowing interlayer phosphate to react with dissolved Fe(II) to form intermediate amorphous Fe(II) phosphates. With time, this amorphous Fe(II) phosphate will likely convert into vivianite. When P and Fe(II) concentrations approach the molar ratio of stoichiometric vivianite, GR does not form as an intermediate phase and crystalline vivianite forms.

In modern oligotrophic ferruginous settings, where P concentrations in the water column are relatively low, GR may be a major mineral forming at the redoxcline (e.g., Zegeye et al., 2012; Halevy et al., 2017). By contrast, in higher P ferruginous settings, Fe(II)-phosphate may be the dominant P-bearing mineral forming in the deeper anoxic waters (Cosmidis et al., 2014). Hence, we suggest that in a global ferruginous ocean where productivity is low through continual removal of P in association with Fe minerals, GR formation should play a substantial role in removing P from solution and maintaining oligotrophic conditions. These environmental conditions were likely prevalent during intervals of the Archean and the early Neoproterozoic (e.g., Poulton and Canfield, 2011; Sperling et al., 2015; Guilbaud et al., 2015). By contrast, when euxinia became more prevalent along productive continental margins, such as during the Neoproterozoic (e.g., Reinhard et al., 2009; Kendall et al., 2010; Zerkle et al., 2012), and at times in the mid-Proterozoic (e.g., Shen et al., 2002; Poulton et al., 2010; Scott et al., 2008), P recycling back to the water column was likely more intense, leading to higher dissolved P concentrations. Under such eutrophic conditions, vivianite precipitation would exert a dominant mineralogical constraint on the extent of P recycling, and hence the bioavailability of P (Derry, 2015).

Declaration of Competing Interest

The authors declare that they have no known competing financial interests or personal relationships that could have appeared to influence the work reported in this paper.

Acknowledgements

This work was supported by a University of Leeds (School of Earth and Environment) research training grant to YX. SWP acknowledges support from a Royal Society Wolfson Research.

Merit Award and NERC grants NE/R010129/1 and NE/T008458/1. We thank the editors, and Lou Derry and two anonymous reviewers for their constructive comments and suggestions.

Appendix A. Supplementary material

Supplementary data to this article includes pH measurements, and dissolved P, dissolved Fe(II), loosely-bound P, loosely-bound Fe(II), solid P and solid Fe concentrations through time, for experiments 1 to 6.

Supplementary data to this article can be found online at <https://doi.org/10.1016/j.gca.2023.04.032>.

References

- Alcott, L.J., Mills, B.J.W., Bekker, A., Poulton, S.W., 2022. Earth's Great Oxidation Event facilitated by the rise of phosphorus recycling. *Nat. Geosci.* 15, 210–215.
- Barthélémy, K., Naille, S., Despas, C., Ruby, C., Mallet, M., 2012. Carbonated ferric green rust as a new material for efficient phosphate removal. *J. Interface Sci.* 384, 121–127.
- Bauer, K.W., Byrne, J., Kenward, P., Simister, R., Michiels, C., Friese, A., Vuillemin, A., Henny, C., Nomosatryo, S., Kallmeyer, J., Kappler, A., Smit, M., Francois, R., Crowe, S.A., 2020. Magnetite biomineralization in ferruginous waters and early Earth evolution. *Earth Planet. Sci. Lett.* 549, 116495.
- Benali, O., Abdelmoula, M., Refait, P., Génin, J.M.R., 2001. Effect of orthophosphate on the oxidation products of Fe(II)-Fe(III) hydroxycarbonate: The transformation of green rust to ferrihydrite. *Geochim. Cosmochim. Acta* 65, 1715–1726.
- Bernal, J.D., Dasgupta, D.T., Mackay, A.L., 1959. The oxides and hydroxides of iron and their structural inter-relationships. *Clay Mineral. Bull.* 4, 15–30.
- Berthelin, J., Ona-Nguema, G., Stemmler, S., Quantin, C., Abdelmo-ula, M., Jorand, F., 2006. Bioreduction of ferric species and biogenesis of green rusts in soils. *Compt. Rendus Geosci.* 338, 447–455.
- Bjerrum, C.J., Canfield, D.E., 2002. Ocean productivity before about 1.9 Gyr ago limited by phosphorus adsorption onto iron oxides. *Nature* 417, 159–162.
- Bocher, F., Génin, A., Ruby, C., Ghanbaja, J., Abdelmoula, M., Génin, J.-M.-R., 2004. Coprecipitation of Fe(II-III) hydroxycarbonate green rust stabilised by phosphate adsorption. *Solid State Sci.* 6, 117–124.
- Bowyer, F.T., Shore, A.J., Wood, R.A., Alcott, L.J., Thomas, A.L., Butler, I.B., Curtis, A., Hainan, S., Curtis-Walcott, S., Penny, A.M., Poulton, S.W., 2020. Regional nutrient decrease drove redox stabilisation and metazoan diversification in the late Ediacaran Nama Group, Namibia. *Sci. Rep.* 10, 2240.
- Busigny, V., Planavsky, N.J., Jézéquel, D., Crowe, S., Louvat, P., Moureau, J., Viollier, E., Lyons, T.W., 2014. Iron isotopes in an Archean ocean analogue. *Geochim. Cosmochim. Acta* 133, 443–462.
- Butler, I.B., Schoonen, A.A., Rickard, D.T., 1994. Removal of dissolved oxygen from water: a comparison of four common techniques. *Talanta* 41, 211–215.
- Canfield, D.E., Bjerrum, C.J., Zhang, S., Wang, H., Wang, X., 2020. The modern phosphorus cycle informs interpretations of Mesoproterozoic Era phosphorus dynamics. *Earth-Sci. Rev.* 208, 103267.
- Canfield, D.E., Rosing, M.T., Bjerrum, C., 2006. Early anaerobic metabolisms. *Phil. Trans. R. Soc. B* 361, 1891–1836.
- Christian, G.D., 2014. In: Christian, G.D., et al. (Eds.), *Analytical chemistry*. John Wiley and Sons, Inc., Hoboken, NJ.
- Cosmidis, J., Benzerara, K., Morin, G., Busigny, V., Lebeau, O., Jézéquel, D., Noël, V., Dublet, G., Othmane, G., 2014. Biomineralization of iron-phosphates in the water column of Lake Pavin (Massif Central, France). *Geochim. Cosmochim. Acta* 126, 78–96.
- Crowe, S.A., 2008. The biogeochemistry of tropical lakes: A case study from Lake Matano, Indonesia. *Limnol. Oceanogr.* 53, 319–331.
- Crowe, S.A., Jones, C., Katsev, S., Magen, C., O'Neill, A.H., Sturm, A., Canfield, D.E., Haffner, G.D., Mucci, A., Sundby, B., Fowle, D.A., 2008. Photoferrotrophs thrive in an Archean Ocean analogue. *Proc. Natl. Acad. Sci.* 105, 15938–15943.
- Dellwig, O., Leippe, T., März, C., Glockzin, M., Pollehn, F., Schmetzger, B., Yakushev, E.V., Boettcher, M.E., Brumsack, H., 2010. A new particulate Mn-Fe-P-shuttle at the redoxcline of anoxic basins. *Geochim. Cosmochim. Acta* 74, 7100–7115.
- Derry, L.A., 2015. Causes and consequences of mid-Proterozoic anoxia. *Geophys. Res. Lett.* 42, 8538–8546.
- Dijkstra, N., Slomp, C.P., Behrends, T., 2016. Expedition 347 Scientists, Vivianite is a key sink for phosphorus in sediments of the Landsort Deep, an intermittently anoxic deep basin in the Baltic Sea. *Chem. Geol.* 438, 58–72.
- Dijkstra, N., Kraal, P., Séguret, M.J.M., Flores, M.R., Gonzalez, S., Rijkenberg, M.J.A., Slomp, C.P., 2018. Phosphorus dynamics in and below the redoxcline in the Black Sea and implications for phosphorus burial. *Geochim. Cosmochim. Acta* 222, 685–703.
- Egger, M., Jilbert, T., Behrends, T., Rivard, C., Slomp, C.P., 2015. Vivianite is a major sink for phosphorus in methanogenic coastal surface sediments. *Geochim. Cosmochim. Acta* 169, 217–235.
- Etique, M., Jorand, F.P.A., Zegeye, A., Grégoire, B., Despas, C., Ruby, C., 2014. Abiotic process for Fe(II) oxidation and green rust mineralization driven by a heterotrophic nitrate reducing bacteria (*Klebsiella mobilis*). *Environ. Sci. Technol.* 48, 3742–3751.
- Fredrickson, J.K., Zachara, J.M., Kennedy, D.W., Dong, H., Onstott, T.C., Hinman, N.W., Li, S.-M., 1998. Biogenic iron mineralization accompanying the dissimilatory reduction of hydrous ferric oxide by a groundwater bacterium. *Geochim. Cosmochim. Acta* 62, 3239–3257.
- Gálvez, N., Barrón, V., Torrent, J., 1999. Effect of phosphate on the crystallization of hematite, goethite, and lepidocrocite from ferrihydrite. *Clays Clay Miner.* 47, 304–311.
- Guilbaud, R., White, M., Poulton, S.W., 2013. Surface charge and growth of sulphate and carbonate green rust in aqueous media. *Geochim. Cosmochim. Acta* 108, 141–153.
- Guilbaud, R., Poulton, S.W., Butterfield, N.J., Zhu, M., Shields-Zhou, G.A., 2015. A global transition to ferruginous conditions in the early Neoproterozoic oceans. *Nat. Geosci.* 8, 466–470.
- Guilbaud, R., Poulton, S.W., Thompson, J., Husband, K.F., Zhu, M., Zhou, Y., Shields, G.A., Lenton, T.M., 2020. Phosphorus-limited conditions in the early Neoproterozoic Ocean maintained low levels of atmospheric oxygen. *Nat. Geosci.* 13, 296–301.
- Halevy, I., Alesker, M., Schuster, E.M., Popovitz-Biro, R., Feldman, Y., 2017. A key role for green rust in the Precambrian oceans and the genesis of iron formations. *Nat. Geosci.* 10, 135–139.
- Hansen, H.C.B., 1989. Composition, stabilization, and light adsorption of Fe(II)Fe(III) hydroxycarbonate (green rust). *Clay Miner.* 24, 663–669.
- Hansen, H.C.B., Poulsen, I.F., 1999. Interaction of synthetic sulphate “green rust” with phosphate and the crystallization of vivianite. *Clays Clay Miner.* 47, 312–318.
- Hsu, T., Jiang, W., Wang, Y., 2014. Authigenesis of vivianite as influenced by methane-induced sulfidation in cold-seep sediments off southwestern Taiwan. *J. Asian Earth Sci.* 89, 88–97.
- Ingall, E.D., Jahnke, R.A., 1997. Influence of water-column anoxia on the elemental fractionation of carbon and phosphorus during sediment diagenesis. *Mar. Geol.* 139, 219–229.
- Ingall, E.D., Bustin, R.M., Van Cappellen, P., 1993. Influence of water column anoxia on the burial and preservation of carbon and phosphorus in marine shales. *Geochim. Cosmochim. Acta* 57, 303–316.
- Jenkyns, H.C., 2010. Geochemistry of oceanic anoxic events. *Geochem., Geophys. Geosyst.* 11, 1–30.
- Jones, C., Nomosatryo, S., Crowe, S.A., Bjerrum, C.J., Canfield, D.E., 2015. Iron oxides, divalent cations, silica, and the early earth phosphorus crisis. *Geology* 43, 135–138.
- Jorand, F.P.A., Sergent, A.-S., Remy, P.-P., Bihannic, I., Ghanbaja, J., Lartiges, B., Hanna, K., Zegeye, A., 2013. Contribution of anionic vs neutral polymers to the formation of green rust 1 from γ -FeOOH bioreduction. *Geomicrobiol. J.* 30, 1–16.
- Kappler, A., Newman, D.K., 2004. Formation of Fe(III)-minerals by Fe(II)-oxidizing photoautotrophic bacteria. *Geochim. Cosmochim. Acta* 68, 1217–1226.
- Kendall, B., Reinhard, C.T., Lyons, T.W., Kaufman, A.J., Poulton, S.W., Anbar, A.D., 2010. Pervasive oxygenation along late Archean ocean margins. *Nat. Geosci.* 3, 647–652.
- Koeksoy, E., Sundman, A., Byrne, J.M., Lohmayer, R., Planer-Friedrich, B., Halevy, I., Konhauser, K.O., Kappler, A., 2019. Formation of green rust and elemental sulfur in an analogue for oxygenated ferro-euxinic transition zones of Precambrian oceans. *Geology* 47, 211–214.
- Konhauser, K.O., Amskold, L., Lalonde, S.V., Posth, N.R., Kappler, A., Anbar, A., 2007a. Decoupling photochemical Fe(II) oxidation from shallow-water BIF deposition. *Earth Planet. Sci. Lett.* 258, 87–100.
- Konhauser, K.O., Lalonde, S.V., Amskold, L., Holland, H.D., 2007b. Was there really an Archean phosphate crisis? *Science* 315, 1234.
- Koroleff, F., 1976. Determination of phosphorus. In: Grasshoff, K. (Ed.), *Methods of seawater analysis*, 2nd ed. Verlag Chemie, Weinheim, pp. 117–156.
- Krom, M.D., Berner, R.A., 1980. Adsorption of phosphate in anoxic marine sediments. *Limnol. Oceanogr.* 25, 797–806.
- Krom, M.D., Berner, R.A., 1981. The diagenesis of phosphorus in a nearshore marine sediment. *Geochim. Cosmochim. Acta* 45, 207–216.
- Kubeneck, L.J., Lenstra, W.K., Malkin, S.Y., Conley, D.J., Slomp, C.P., 2021. Phosphorus burial in vivianite-type minerals in methane-rich coastal sediments. *Mar. Chem.* 231, 103948.
- Kukkadapu, R.K., Zachara, J.M., Fredrickson, J.K., Kennedy, D.W., 2004. Biotransformation of two-line silica-ferrihydrite by a dissimilatory Fe(III)-reducing bacterium: formation of carbonate green rust in the presence of phosphate. *Geochim. Cosmochim. Acta* 68, 2799–2814.
- Laakso, T.A., Schrag, D.P., 2014. Regulation of atmospheric oxygen during the Proterozoic. *Earth Planet. Sci. Lett.* 388, 81–91.
- Li, Y.-L., Konhauser, K.O., Zhai, M., 2017. The formation of magnetite in the early Archean oceans. *Earth. Planet. Sci. Lett.* 466, 103–114.
- März, C., Hoffmann, J., Bleil, U., de Lange, G.J., Kasten, S., 2008. Diagenetic changes of magnetic and geochemical signals by anaerobic methane oxidation in sediments of the Zambesi deep-sea fan (SW Indian Ocean). *Mar. Geol.* 255, 118–130.
- Madsen, H.E.L., Hansen, H.C.B., 2014. Kinetics of crystal growth of vivianite, $\text{Fe}_3(\text{PO}_4)_2 \cdot 8\text{H}_2\text{O}$, from solution at 25, 35 and 45°C. *J. Cryst. Growth* 401, 82–86.
- Mori, H., Ito, T., 1950. The structure of vivianite and symplectite. *Acta Crystallogr.* 3, 1–6.
- Nriagu, J.O., 1984. *Phosphate Minerals: Their properties and General Modes of Occurrence*. In: Nriagu, J.O., Moore, P.B. (Eds.), *Phosphate minerals*. Springer, Berlin, pp. 126.
- O'Connell, D.W., Jensen, M.M., Jakobsen, R., Thamdrup, B., Andersen, T.J., Kovacs, A., Hansen, H.C.B., 2015. Vivianite formation and its role in phosphorus retention in Lake Ørn, Denmark. *Chem. Geol.* 409, 42–53.
- O'Loughlin, E.J., Larese-Casanova, P., Scherer, M., Cook, R., 2007. Green rust formation from the bioreduction of γ -FeOOH (lepidocrocite): comparison of several *Shewanella* species. *Geomicrobiol. J.* 24, 211–230.
- Ona-Nguema, G., Jorand, F., Benali, O., Abdelmoula, M., Génin, J.-M.R., Block, J.-C., 2001. Key role of the kinetics of γ -FeOOH bioreduction on the Formation of Fe(II-III) minerals. In: Thomas, M.F., et al. (Eds.), *Hyperferrous Interactions (C): Proceedings of the International Conference on the Applications of the Mössbauer Effect*. Dordrecht, The Netherlands, pp. 415–418.
- Ona-Nguema, G., Carteret, C., Benali, O., Abdelmoula, M., Génin, J.M., Jorand, F., 2004. Competitive formation of hydroxycarbonate green rust 1 versus hydroxysulphate green rust 2 in *Shewanella putrefaciens* cultures. *Geomicrobiol. J.* 21, 79–90.
- Pantke, C., Obst, M., Benzerara, K., Morin, G., Ona-Nguema, G., Dippon, U., Kappler, A., 2012. Green rust formation during Fe(II) oxidation by the nitrate-reducing *Acidovorax* sp. strain BoFeN1. *Environ. Sci. Technol.* 46, 1439–1446.
- Peiffer, S., Dos Santos Afonso, M., Wehrl, B., Gaechter, R., 1992. Kinetics and mechanism of the reaction of H_2S with lepidocrocite. *Environ. Sci. Technol.* 26, 2408–2413.
- Poulton, S.W., 2017. Early phosphorus redigested. *Nat. Geosci.* 10, 75–76.
- Poulton, S.W., 2003. Sulfide oxidation and iron dissolution kinetics during the reaction of dissolved sulfide with ferrihydrite. *Chem. Geol.* 202, 79–94.

- Poulton, S.W., Canfield, D.E., 2011. Ferruginous conditions: A dominant feature of the ocean through Earth's history. *Elements* 7, 107–112.
- Poulton, S.W., Krom, M.D., Raiswell, R., 2004. A revised scheme for the reactivity of iron (oxyhydr)oxide minerals towards dissolved sulfide. *Geochim. Cosmochim. Acta* 68, 3703–3715.
- Poulton, S.W., Fralick, P.W., Canfield, D.E., 2010. Spatial variability in oceanic redox structure 1.8 billion years ago. *Nat. Geosci.* 3, 486–498.
- Poulton, S.W., Henkel, S., März, C., Urquhart, H., Flögel, S., Kasten, S., Sinninghe Damsté, J.S., Wagner, T., 2015. A continental-weathering control on orbitally driven redox-nutrient cycling during Cretaceous Oceanic Anoxic Event 2. *Geology* 43, 963–966.
- Planavsky, N.J., Rouxel, O.J., Bekker, A., Lalonde, S.V., Konhauser, K.O., Reinhard, C.T., Lyons, T.W., 2010. The evolution of the marine phosphate reservoir. *Nature* 467, 1088–1090.
- Pyzik, A.J., Sommer, S.E., 1981. Sedimentary iron monosulfides: Kinetics and mechanism of formation. *Geochim. Cosmochim. Acta* 45, 687–698.
- Randall, S.R., Sherman, D.M., Ragnarsdóttir, K.V., 2001. Sorption of As(V) on green rust (Fe₄(II)Fe₂(III)(OH)₁₂SO₄•3H₂O) and lepidocrocite (c-FeOOH): surface complexes from EXAFS spectroscopy. *Geochim. Cosmochim. Acta* 65, 1015–1023.
- Refait, P., Drissi, S.H., Pytkiewicz, J., Génin, J.-M.-R., 1997. The anionic species competition in iron aqueous corrosion: role of various green rust compounds. *Corr. Sci.* 39, 1699–1710.
- Refait, P., Abdelmoula, M., Génin, J.-M.-R., 1998. Mechanisms of formation and structure of green rust one in aqueous corrosion of iron in the presence of chloride ions. *Corros. Sci.* 40, 1547–1560.
- Reinhard, C.T., Raiswell, R., Scott, C., Anbar, A.D., Lyons, T.W., 2009. A Late Archean sulfidic sea stimulated by early oxidative weathering of the continents. *Science* 326, 713–716.
- Reinhard, C.T., Planavsky, N.J., Gill, B.C., Ozaki, K., Robbins, L.J., Lyons, T.W., Fischer, W.W., Wang, C., Cole, D.B., Konhauser, K.O., 2017. Evolution of the global phosphorus cycle. *Nature* 541, 386–401.
- Rothe, M., Frederichs, T., Eder, M., Kleeberg, A., Hupfer, M., 2014. Evidence for vivianite formation and its contribution to long-term phosphorus retention in a recent lake sediment: a novel analytical approach. *Biogeosciences* 11, 5169–5180.
- Ruby, C., Géhin, A., Abdelmoula, M., Génin, J.-M.-R., Jolivet, J.-P., 2003. Coprecipitation of Fe(II) and Fe(III) cations in sulphated aqueous medium and formation of hydroxysulphate green rust. *Solid State Sci.* 5, 1055–1062.
- Ruby, C., Aïssa, R., Géhin, A., Cortot, J., Abdelmoula, M., Génin, J.-M.-R., 2006. Green rusts synthesis by coprecipitation of Fe^{II}–Fe^{III} ions and mass-balance diagram. *C. -R. Geosci.* 338, 420–432.
- Ruttenberg, K.C., 1992. Development of a sequential extraction method for different form of phosphorus in marine sediments. *Limnol. Oceanogr.* 37, 1460–1482.
- Scott, C.T., Lyons, T.W., Bekker, A., Shen, Y., Poulton, S.W., Chu, X., Anbar, A.D., 2008. Tracing the stepwise oxygenation of the Proterozoic ocean. *Nature* 452, 456–459.
- Schwertmann, U., Fechter, H., 1994. The formation of green rust and its transformation to lepidocrocite. *Clay Miner.* 29, 87–92.
- Shen, Y., Canfield, D.E., Knoll, A.H., 2002. Middle Proterozoic ocean chemistry: evidence from the McArthur Basin, northern Australia. *Am. J. Sci.* 302, 81–109.
- Simon, L., François, M., Refait, P., Renaudin, G., Lelaurain, M., Génin, J.-M.-R., 2003. Structure of the Fe(II–III) layered double hydroxysulphate green rust two from Rietveld analysis. *Solid State Sci.* 5, 327–334.
- Slomp, C.P., Thomson, J., de Lange, G.J., 2004. Controls on phosphorus regeneration and burial during formation of eastern Mediterranean sapropels. *Mar. Geol.* 203, 141–159.
- Slomp, C.P., Mort, H.P., Jilbert, T., Reed, D.C., Gustafsson, B.G., Wolthers, M., 2013. Coupled dynamics of iron and phosphorus in sediments of an oligotrophic coastal basin and the impact of anaerobic oxidation of methane. *PLoS ONE* 8, e62386.
- Sperling, E.A., Wolock, C.J., Morgan, A.S., Gill, B.C., Kunzmann, M., Halverson, G.P., Macdonald, F.A., Knoll, A.H., Johnston, D.T., 2015. Statistical analysis of iron geochemical data suggests limited late Proterozoic oxygenation. *Nature* 523, 451–454.
- Stookey, L.L., 1970. Ferrozine-A new spectrophotometric reagent for iron. *Anal. Chem.* 42, 779–781.
- Sumoondur, A., Shaw, S., Ahmed, I., Benning, L.G., 2008. Green rust as a precursor for magnetite: an in situ synchrotron based study. *Mineral. Mag.* 72 (1), 201–204.
- Turnewitsch, R., Pohl, C., 2010. An estimate of the efficiency of the iron- and manganese-driven dissolved inorganic phosphorus trap at an oxic/euxinic water column redoxcline. *Global Biogeochem. Cycles* 24, GB4025.
- Tyrrill, T., 1999. The relative influences of nitrogen and phosphorus on oceanic primary production. *Nature* 400, 525–531.
- Usman, M., Abdelmoula, M., Hanna, K., Grégoire, B., Faure, P., Ruby, C., 2012. Fe^{II} induced mineralogical transformations of ferric oxyhydroxides into magnetite of variable stoichiometry and morphology. *J. Solid State Chem.* 194, 328–335.
- Van Cappellen, P., Ingall, E.D., 1994. Benthic phosphorus regeneration, net primary production, and ocean anoxia: A model of the coupled marine biogeochemical cycles of carbon and phosphorus. *Paleoceanogr.* 9, 677–692.
- Viollier, E., Hunter, K., Roychoudhury, A.N., van Cappellen, P., 2000. The ferrozine method revisited: Fe(II)/Fe(III) determination in natural waters. *Appl. Geochem.* 15, 785–790.
- Vuillemin, A., Friese, A., Alawi, M., Henny, C., Nomosatryo, S., Wagner, D., Crowe, S.A., Kallmeyer, J., 2016. Geomicrobiological features of ferruginous sediments from Lake Towuti, Indonesia. *Front. Microbiol.* 7, e1007.
- Vuillemin, A., Wirth, R., Kemnitz, H., Schleicher, A.M., Fiese, A., Bauer, K.W., Simister, R., Nomosatryo, S., Ordoñez, L., Ariztegui, D., Henny, C., Crowe, S.A., Benning, L.G., Kallmeyer, J., Russell, J.M., Bijaksana, S., Vogel, H., and the Towuti Drilling Project Science team, 2019. Formation of diagenetic siderite in modern ferruginous sediments. *Geology* 47, 541–544.
- Vuillemin, A., Friese, A., Wirth, R., Schuessler, J.A., Schleicher, A.M., Kemnitz, H., Lücke, A., Bauer, K.W., Nomosatryo, S., von Blanckenburg, F., Simister, R., Ordoñez, L.G., Ariztegui, D., Henny, C., Russell, J.M., Bijaksana, S., Vogel, H., Crowe, S.A., Kallmeyer, J., and the Towuti Drilling Project Science team, 2020. Vivianite formation in ferruginous sediments from Lake Towuti, Indonesia. *Biogeosciences* 17, 1955–1973.
- Xiong, Y., Guilbaud, R., Peacock, C.L., Cox, R.P., Canfield, D.E., Krom, M.D., Poulton, S.W., 2019. Phosphorus cycling in Lake Cadagno, Switzerland: a low sulfate euxinic ocean analogue. *Geochim. Cosmochim. Acta* 251, 116–135.
- Zegeye, A., Ruby, C., Jorand, F., 2007a. Kinetic and thermo-dynamic analysis during dissimilatory-FeOOH reduction: formation of green rust 1 and magnetite. *Geomicrobiol. J.* 24, 51–64.
- Zegeye, A., Huguet, L., Abdelmoula, M., Carteret, C., Mullet, M., Jorand, F., 2007b. Biogenic hydroxysulfate green rust, a potential electron acceptor for SRB activity. *Geochim. Cosmochim. Acta* 71, 5450–5462.
- Zegeye, A., Bonneville, S., Benning, L.G., Sturm, A., Fowle, D.A., Jones, C., Canfield, D.E., Ruby, C., MacLean, L.C., Nomosatryo, S., Crowe, S.A., Poulton, S.W., 2012. Green rust formation controls nutrient availability in a ferruginous water column. *Geology* 40, 599–602.
- Zerkle, A.L., Claire, M., Domagal-Goldman, S.D., Farquhar, J., Poulton, S.W., 2012. A bistable organic-rich atmosphere on the Neoproterozoic Earth. *Nat. Geosci.* 5, 359–363.